Electron beam induced oxidation of surfaces of Ni3Al-base alloys

Koch, S.A.; Agterveld, D.T.L.van; Palasantzas, G.; de Hosson, J.T.M.

Published in:
Surface Science

DOI:
10.1016/S0039-6028(01)00697-5

Publication date:
2001

ELSEVIER

Surface Science 476 (2001) L267–L272

SURFACE SCIENCE

www.elsevier.nl/locate/susc

Surface Science Letters

Electron beam induced oxidation of surfaces of Ni_3Al-base alloys

S.A. Koch, D.T.L van Agterveld, G. Palasantzas, J.Th.M. De Hosson *

Department of Applied Physics, Materials Science Center, The Netherlands Institute for Metals Research, University of Groningen, Nijenborgh 4, 9747 AG Groningen, The Netherlands

Received 11 July 2000; accepted for publication 2 January 2001

Abstract

This letter concentrates on phenomena of the electron beam (e-beam) induced oxidation of surfaces of Ni_3Al-base alloys. In particular it is shown that an e-beam may contribute substantially to the oxidation behavior of polycrystalline Ni_3Al and Ni_3Al–B surfaces during Auger analysis at room temperature. Upon e-beam exposure oxidation occurs rapidly, even though any regime of oxygen chemisorption is absent. Auger peak-to-peak oxygen curves for Ni_3Al(–B) surfaces appear to support the model by Li et al. [J. Vac. Sci. Technol. A 13 (1995) 1574] based on the premise that the e-beam creates additional nucleation sites for oxidation. In contrast, for pure Ni containing B in solid solution a chemisorption regime is indeed present which is then followed by a rapid formation of oxides that saturates quickly at a time scale similar to that of the Ni_3Al-base systems. Although Al does not participate in the e-beam induced oxidation, the cross-sections for creation of oxide sites are found to be drastically higher than those of Ni/B and pure Ni.

Keywords: Oxidation; Auger electron spectroscopy; Electron microscopy; Alloys

Fundamental and technological interests in the fields of corrosion and catalysis have given an impetus to numerous investigations on the growth of oxide layers on Ni and Ni/Al alloy surfaces [1–7]. Furthermore, these studies are important for lithography techniques in microelectronic device fabrication [8], exchange-bias junctions [9], aerospace technology [10,11], etc. Notably Ni_3Al alloys have excellent resistance to oxidation because an adherent surface oxide film is formed that protects the base metal from excessive attack [12]. Moreover, B-doped polycrystalline Ni_3Al (~0.1–0.5 at.% B) alloys have been intensively investigated both theoretically and experimentally as potential engineering materials, because B appears to enhance the ductility of polycrystalline alloys at high temperature deformation [12–15].

Although many oxidation studies were performed for Ni [1–7], even so in comparison with electron beam (e-beam) stimulated oxidation [3,4] the oxidation of Ni_3Al(–B) surfaces under the influence of an e-beam remains still unexplored. It is also necessary to properly quantify e-beam effects in B segregation studies, because they may alter strongly the distribution of B on surfaces/interfaces, i.e. in fracture of polycrystalline Ni_3Al alloys

* Corresponding author. Tel.: +31-50-363-4898; fax: +31-50-363-4881.

E-mail address: hossonj@phys.rug.nl (J.Th.M. De Hosson).

0039-6028/01/$ - see front matter
PII: S0039-6028(01)00697-5

under ultra-high-vacuum (UHV) conditions. Indeed, under these conditions and at elevated substrate temperatures exposure to partial O pressure of Ni_3Al leads predominantly to the formation of Al_2O_3 with a structure that depends on the adsorption temperature [16–18]. However, room temperature (RT $\sim$ 300 K) studies have shown that O chemisorbs at Ni sites or mixed Ni/Al sites leading to a disordered surface [18,19] without Al_2O_3 being formed. Moreover, RT scanning tunneling microscopy (STM) studies indicated the formation of small oxide nuclei, i.e. on Ni_3Al (1 1 1) surfaces and an oxide formation that is governed by the mobility of O atoms rather than a substantial transport of metal atoms [19].

In the past the influence of the e-beam on the formation of oxides on pure Ni was analyzed on the premise that electrons create nucleation centers around which oxide islands (NiO) grow [3,4]. Such a premise appears also to be reasonable for Ni_3Al surfaces as the STM studies indicated [19]. Therefore in this work the interaction of molecular O_2 with Ni_3Al(–B) surfaces (held at RT) under the influence of an e-beam will be investigated by in situ scanning Auger/electron microscopy under UHV conditions. Comparison with the oxidation kinetics for pure Ni and Ni with B in solid solution is performed to further exemplify the role of B under e-beam stimulated oxidation.

The apparatus is described in detail elsewhere [20]. It consists of a UHV (base pressure $\sim 4 \times 10^{-8}$ Pa which was used during e-beam induced oxidations) scanning Auger/electron microscope (field emission JEOL JAMP7800F). Moreover, under typical imaging conditions (accelerating voltage 10 keV and e-beam current 2.4 nA, which will be used for all the e-beam induced oxidation that will be presented in this work) the attained minimum beam spot size is $\sim$15 nm which was used for Auger elemental mapping. Hypostoichiometric Ni_3Al–B ($\sim$24 at.% Al) samples were prepared by arc melting with a concentration of $\sim$0.5 at.% B, and homogenized at 1100°C (for 24 h) to form the ordered $L1_2$ (Strukturbericht notation), i.e. Pm3m, structure of Ni_3Al [12–15]. Finally, Ni/B samples which contain patches of Ni with B in solid solution (Ni–B) surrounded by the Ni_3B phase were home made, also using arc melting. The AES measurements were performed on polished cross-sections which were cleaned by Ar^+ sputtering prior to e-beam exposure. Depth profile analyses were performed by Ar^+ sputtering at a rate of $\sim$3.3 nm/min calibrated with respect to Si oxide. The AES data were acquired with 400 ms dwell time (acquisition time/eV). Molecular O_2 was provided by the UHV atmosphere to initiate oxidation.

In the past various oxide growth models which are the starting point of this work described the oxidation of Ni. The island growth oxide model [2,6,7] assumes lateral growth of oxide islands which depends on various parameters such as initial nucleation sites, collision rate of O molecules/atoms with the substrate, as well as the rate constant K_1 for perimeter growth of the oxides. Another model developed by Zion et al. [2] termed hereafter as the Langmuir model, is based on the assumptions that the oxidation growth rate depends on the impingement rate of the oxygen molecules, a Langmuir oxide coverage, and a rate constant. For both models, the O coverage $\Theta(\Phi)$ can be described as $\Theta(\Phi) = \Theta_{\mathrm{sat}} - (\Theta_{\mathrm{sat}} - \Theta_{\mathrm{chem}}) \times \exp[-K_c(\Phi - \Phi_{\mathrm{O}})^c](\Phi > \Phi_{\mathrm{O}})$ with Φ the O exposure, K_c an oxidation rate constant, Θ_{chem} the chemisorption saturation, Θ_{sat} the saturation coverage, and Φ_{O} the oxide onset exposure [2,6,7]. The island growth model has a second-order dependence on Φ or $c = 2$ (growth rate dependence on island perimeter), whereas the Langmuir model has a first-order dependence on Φ or $c = 1$. Li et al. [4] proposed a model for an e-beam induced oxidation that is based on the premise that incident electrons create additional nucleation sites around which oxide islands grow. This model reads of the form [4] $\Theta(t) = \Theta_{\mathrm{sat}} - (\Theta_{\mathrm{sat}} - \Theta_{\mathrm{chem}}) \exp[-kt - (k/\varphi_{\mathrm{e}}\sigma)(\exp(-\varphi_{\mathrm{e}}\sigma t) - 1)]$ with φ_{e} the e-beam density flux, σ the electron energy dependent cross-section for the creation of oxide nucleation sites, t the oxidation time, and k an oxidation rate constant.

Fig. 1 shows e-beam induced oxidation of a (poly-) Ni_3Al–B ($\sim$0.5 at.% B) alloy surface. As the Auger map for O indicates (Fig. 1) the oxidation within the beam area is rather uniform and drastically higher than the surrounding area which was not exposed for a prolonged time (besides for imaging). From the data any initial chemisorption

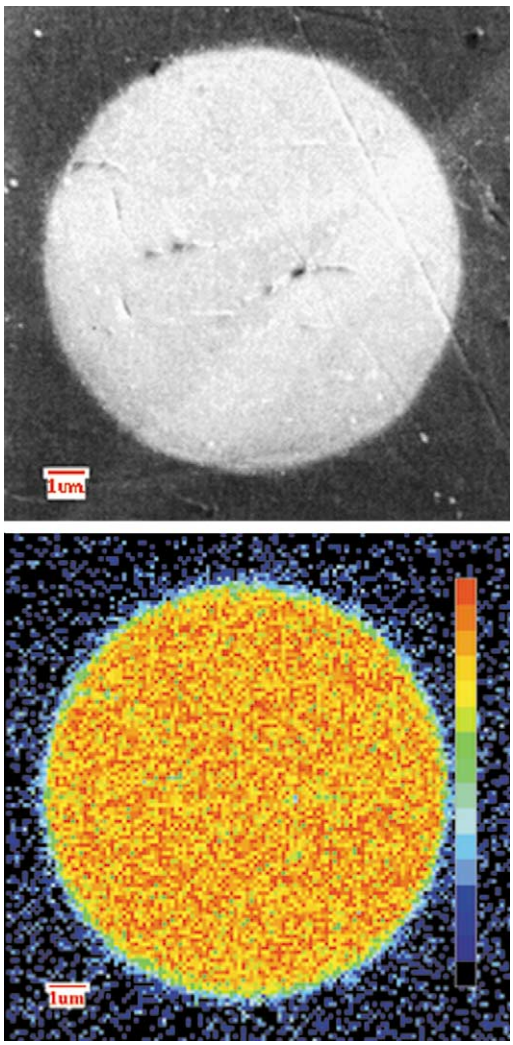

Fig. 1. SEM and SAM images of O after beam induced oxidation on a polished Ni_3Al–B surface. The color bar is indicative of the amount of O. The SAM image shows the ratio $(P - B/B)$ with P the direct spectrum Auger peak intensity and B the background. Accelerating electron voltage 10 keV and e-beam current 2.4 nA.

regime is missing, while fast oxide growth occurs. The O peak-to-peak (p–p) data were fitted initially to the functional form $I(t) = A - (A - B)\exp \times [-(t/\tau)^c]$ with an effective oxidation time τ. [1] The best fit to the O data (Fig. 2; after averaging over three spots that were oxidized sequentially) yielded a characteristic exponent $c^{O}_{Ni_3Al\text{–}B} = 1.23 \pm 0.02$ and an effective oxidation time $\tau^{O}_{Ni_3Al\text{–}B} = 182.8$ min. Depth profile analysis on an oxidized spot shows a significant oxide depth of the order of ≈4–5 nm. Fig. 3 shows oxidation of an undoped (poly)-Ni_3Al surface (averaged over three spots). Again the chemisorption regime is absent, while oxidation proceeds rapidly from the beginning of e-beam exposure. The best fit to the O curve yielded $c^{O}_{Ni_3Al} = 1.27 \pm 0.03$, and $\tau^{O}_{Ni_3Al} = 161.3$ min, i.e. close to the parameters of Ni_3Al–B surfaces.

Based on these results we may disregard the island growth model [6,7] as well as the Langmuir growth model [2] because the exponents are $1 < c^{O}_{Ni_3Al\text{–}B}, c^{O}_{Ni_3Al} < 2$. On the other hand the best fit to the model by Li et al. [4] of the form $I_O(t) = A - (A - B)\exp\,[-kt - (k/\varphi_e\sigma)\{\exp(-\varphi_e\sigma t) - 1\}]$ yields for Ni_3Al–B surfaces $1/k_{Ni_3Al\text{–}B} = 148.6$ min and $(\varphi_e\sigma)_{Ni_3Al\text{–}B} = 2.7 \times 10^{-2}$ min^{-1} (Fig. 2, squares), and for Ni_3Al surfaces $1/k_{Ni_3Al} = 135.9$ min and $(\varphi_e\sigma)_{Ni_3Al} = 3.2 \times 10^{-2}$ min^{-1} (Fig. 3, squares). Both systems (Ni_3Al(–B)) appear rather indistinguishable also in terms of the model by Li et al. [4]. Furthermore, we may estimate the cross-section for the creation of oxide nucleation sites. For the e-beam current 2.4 nA ($1\,A = 6.25 \times 10^{18}$ e^-/s) over an area $\approx \pi d^2/4$ with $d = 10$ μm, the current flux density is $\varphi_e = 1.9 \times 10^{20}$ $e^-/m^2 s$. From the values for $(\varphi_e\sigma)_{Ni_3Al(\text{–}B)}$ we obtain the cross-sections for oxide nucleation centers, namely $\sigma_{Ni_3Al\text{–}B} = 2.4 \times 10^{-24}$ m^2 and $\sigma_{Ni_3Al} = 2.8 \times 10^{-24}$ m^2. Although, these values are significantly smaller than those for pure Ni held at 120 K [4] they are in agreement with the fact that the e-beam effect becomes more pronounced for Ni at lower temperatures [4], whereas at RT island growth has been observed [4,6,7]. Indeed, as the inset of Fig. 3 indicates, the fit by the model of Li et al. yields for pure Ni at RT, $1/k_{Ni} = 174$ min and $(\varphi_e\sigma)_{Ni} = 2.3 \times 10^{-3}$ min^{-1} ($\ll(\varphi_e\sigma)_{Ni_3Al(\text{–}B)}$). The latter for the same current 2.4 nA over an area with a diameter of $d = 5$ μm yields a site creation cross-section $\sigma_{Ni} = 5 \times 10^{-26}$ m^2 ($\ll\sigma_{Ni_3Al(\text{–}B)}$) which is smaller than that of Ni_3Al(–B) by two orders of magnitude.

The Al by itself does not participate on the e-beam induced oxidation at RT (Fig. 2), while for

[1] See Refs. [6,7] and also Figs. 2 and 3 for O-peak intensity vs. O sticking coefficient.

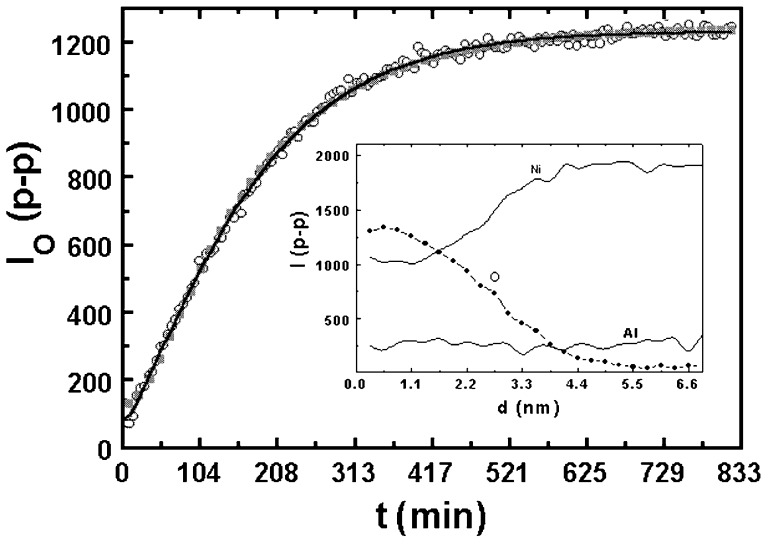

Fig. 2. Evolution of oxygen, acquired with a beam spot size 10 μm and averaged over the three spots. The solid line represents the exponential fit, and squares refer to the model of Ref. [4]. The inset shows a depth profile on an oxidized spot with e-beam spot size of 5 μm. Accelerating electron voltage 10 keV and e-beam current 2.4 nA.

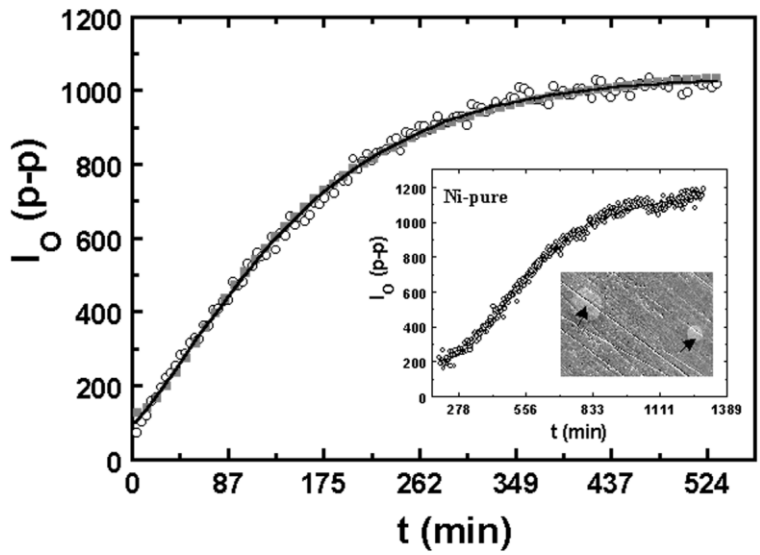

Fig. 3. E-beam oxidation of an undoped Ni_3Al surface in a manner similar to that of Fig. 1. The SEM inset shows the case of pure Ni with two spot sizes 5 and 10 μm. Accelerating electron voltage 10 keV and e-beam current 2.4 nA.

Ni surfaces with B in solid solution (Ni–B) the effect maybe different: Ni–B are the bright areas in Fig. 4 (inset), while the Ni_3B phase is the dark area. The initial chemisorption regime in Fig. 4 (bottom inset) is well fitted to a Langmuir type expression ($c = 1$) yielding an effective chemisorption time $\tau^{OC}_{Ni-B} = 25$ min. Because $\tau^{OC}_{Ni-B} = N_O/2\dot{I}$ [6,7] with the chemisorption centers $N_O \approx 4 \times 10^{18}$ m^{-2} [6,7] we estimate an impingement rate of O_2 molecules of $\dot{I} \approx 1.33 \times 10^{15}$ $m^{-2}\,s^{-1}$ which is

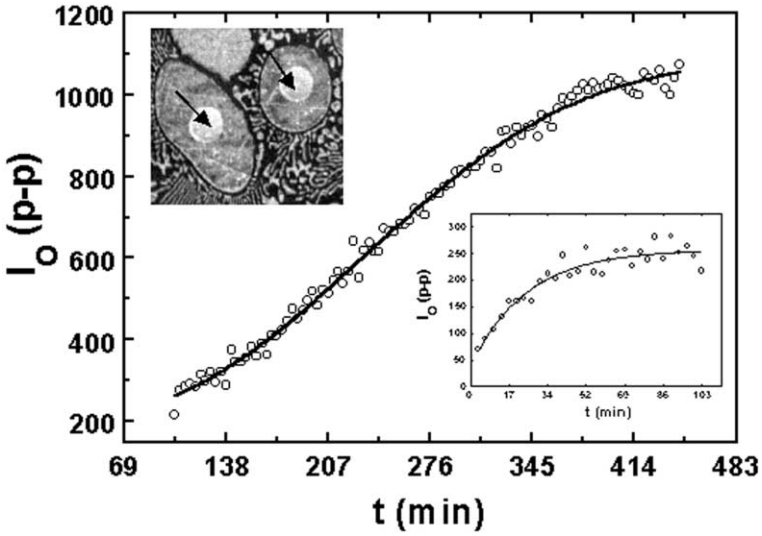

Fig. 4. Beam oxidation of a Ni–B surface. The O curve deviates from the island growth model as the fit indicates. AES data were acquired with a beam spot size of 5 μm (upper inset, bright spots). The chemisorption is shown in the bottom inset. Accelerating electron voltage 10 keV and e-beam current 2.4 nA.

similar to that for pure Ni. Furthermore, the fit to the model of Li et al. [4] yields for the fast oxide growth regime $1/k_{\mathrm{Ni–B}} = 111.6$ min and $(\varphi_e\sigma)_{\mathrm{Ni–B}} = 5 \times 10^{-3}$ min^{-1}. The latter for the same current 2.4 nA over an area with a diameter $d =$ 5 μm (used for Ni–B) yields a site creation cross-section $\sigma_{\mathrm{Ni–B}} = 1.1 \times 10^{-25}$ m^2 which is smaller than that of Ni_3Al(–B). The creation cross-section is approximately one order of magnitude smaller but larger than that of pure Ni. Fast oxide growth occurs at a time scale similar to that of Ni_3Al(–B), whereas the Ni_3B remains almost intact by the e-beam. Depth profile analysis with an e-beam spot size of ~15 nm showed an oxide depth of ≈2–3 nm which is smaller than that of Ni_3Al–B.

Clearly, the oxidation kinetics for Ni_3Al(–B) surpasses any initial chemisorption regime and fast oxide growth prevails. Such an oxidation scenario has been observed also on other systems with high affinity to O, e.g. Al(1 1 1) [21], and Mg(0 0 0 1) [22] where oxide nucleation occurs long before the saturation of a chemisorbed coverage is reached. The oxide nucleation sites are likely to be some type of electron rich site similar to F-center anion vacancies created by sputtering a NiO surface. These sites have shown evidence of dissociative adsorption of molecular O_2 [3]. In addition, electron impact can also cause dissociation of adsorbed water to form OH groups, which catalyze the oxidation on the surface [3]. Note that the direct formation of oxide nucleation centers on Ni_3Al, as was also indicated by STM studies at RT [19], is in agreement with our observation that any chemisorption is negligible whereas fast oxide growth takes place. The fits to the model of Li et al. [4] support the description of e-beam induced nucleation centers around which oxide islands grow. The latter is also manifest in the drastically higher oxide site creation cross-sections than those of Ni–B and pure Ni (closely by one and two orders of magnitude respectively; $\sigma_{\mathrm{Ni_3Al–B}} > \sigma_{\mathrm{Ni–B}}$ and $\sigma_{\mathrm{Ni_3Al–B}} \gg \sigma_{\mathrm{Ni}}$).

Without the effect of the e-beam B segregates to the surface both in Ni_3Al–B and Ni–B surfaces because of its high affinity to O and the Ni enrichment of the surface [23,24]. However, under subsequent exposure to an e-beam NiO continues to develop on the pre-oxidized surface, whereas the B peak decreases rather quickly without any participation of Al in the oxidation process. This e-beam effect on B appears as long as it stays interstitially in the Ni matrix, whereas a compound

in the form Ni_3B strongly resists e-beam induced oxidation. Finally, if we compare the fast oxide growth for Ni_3Al(–B) (prior to saturation) with that of Ni at low temperatures (147 K) where any chemisorption is suppressed [6,7], the O sticking coefficient should remain close to 1. However, for pure Ni and Ni–B in the chemisorption regime the O sticking coefficient (at ~300 K) should reduce significantly below 0.1 as long as the chemisorption saturation is reached, and it will remain below 0.1 even when the fast oxide growth commences [6,7].

In conclusion, under the influence of an e-beam Ni_3Al(–B) oxidizes rather quickly due to the creation of oxide nucleation centers as is in agreement with the model proposed by Li et al. [4]. This is also supported by the fact that the exponents obtained from fits to Langmuir/island type models ($1 < c^{O}_{Ni_3Al–B} \leqslant c^{O}_{Ni_3Al} < 2$) exclude either one of them as the principal oxide growth mechanism. Although Al does not participate in the oxidation process at RT, the Ni_3Al(–B) surfaces are more susceptible to e-beam induced NiO formation, with oxide site creation cross-sections significantly higher than those of Ni–B and for pure Ni surfaces. Special care should be taken in boron segregation studies onto Ni_3Al–B surfaces/interfaces with Auger microscopy because of irreversible structural changes associated with an intense Ni oxide formation by the e-beam. Further studies are in progress with different e-beam spot sizes in order to illustrate the effect of different e-beam fluxes φ_e [25].

Acknowledgements

We would like to acknowledge support from the Netherlands Institute for Metals Research and the "Stichting voor Fundamenteel Onderzoek der Materie" (FOM) which is financially supported by the "Nederlandse Organisatie voor Wetenschappelijk Onderzoek (NWO)".

References

[1] J.A. Slezak, B.D. Zion, S.J. Sibener, Surf. Sci. 442 (1999) L983.
[2] B.D. Zion, A.T. Hanbicki, S.J. Sibener, Surf. Sci. 417 (1998) L1154.
[3] M.J. Stirniman, W. Li, S.J. Sibener, J. Chem. Phys. 103 (1995) 451.
[4] W. Li, M.J. Stirniman, S.J. Sibener, J. Vac. Sci. Technol. A 13 (1995) 1574.
[5] W. Li, M.J. Stirniman, S.J. Sibener, Surf. Sci. 329 (1995) L593.
[6] P.H. Holloway, J.B. Hudson, Surf. Sci. 43 (1974) 123.
[7] P.H. Holloway, J.B. Hudson, Surf. Sci. 43 (1974) 141.
[8] E.S. Snow, P.M. Campbell, F.K. Perkins, Naval Res. Rev. XLIX (1997) 15.
[9] J. Noguess, I.K. Shuller, J. Mag. Mag. Mater. 192 (1998) 203.
[10] S.J. Sibener, R.J. Buss, C.Y. Ng, Y.T. Lee, Rev. Sci. Instrum. 51 (1980) 167.
[11] P.N. Peters, H.C. Grogory, J.T. Swann, Appl. Opt. 25 (1986) 1290.
[12] N.S. Stoloff, V.K. Sikka (Eds.), Physical Metallugy and Processing of Intermetallic Compounds, Chapman and Hall, New York, 1996.
[13] B.J. Pestman, J.Th.M. De Hosson, V. Vitek, F.W. Schapink, Philos. Mag. A 64 (1991) 951–969.
[14] J.Th.M. De Hosson, B.J. Pestman, Mater. Sci. Engng. A 164 (1993) 415.
[15] B.J. Pestman, J.Th.M. De Hosson, Acta Metall. Mater. 40 (1992) 2511.
[16] E.W.A. Young, J.C. Rivière, L.S. Welch, Appl. Surf. Sci. 28 (1987) 7.
[17] A.M. Venezia, C.M. Loxton, Surf. Interface Anal. 2 (1988) 287.
[18] C. Becker, J. Kandler, H. Raaf, R. Linke, T. Pelster, M. Dräger, M. Tanemura, K. Wandelt, J. Vac. Sci. Technol. A 16 (1998) 1000.
[19] A. Rosenhahn, J. Schneider, J. Kandler, C. Becker, K. Wandelt, Surf. Sci. 433–435 (1999) 705.
[20] D.T.L. van Agterveld, G. Palasantzas, J.Th.M. De Hosson, Act. Mater. 48 (2000) 1995.
[21] H. Brune, J. Wintterlin, J. Frost, G. Ertl, J. Wiechers, R.J. Behm, J. Chem. Phys. 99 (1993) 2128.
[22] P.A. Thiry, J. Ghijsen, R. Sporken, J.J. Pireaux, R.L. Johnson, R. Caudano, Phys. Rev. B 39 (1989) 3620.
[23] S. Hofmann, M.G. Stepanova, Appl. Surf. Sci. 90 (1995) 227.
[24] S.A. Koch, D.T.L. van Agterveld, G. Palasantzas, J.Th.M. De Hosson, J. Mater. Res., submitted for publication.
[25] G. Palasantzas, D.T.L. van Agterveld, S.A. Koch, J.Th.M. De Hosson, J. Vac. Sci. Technol. B (2000), submitted.